A Robust Half-Cycle Single-Phase Prefiltered Open-Loop Frequency Estimator for Fast Tracking of Amplitude and Phase

Verma, Anant Kumar; Roncero-Sánchez, Pedro ; Ahmed, Hafiz; Elghali, Seifeddine Ben ; Busarello, Tiago Davi Curi

IEEE Transactions on Instrumentation and Measurement

DOI:
https://doi.org/10.1109/TIM.2021.3129211

Published: 02/03/2022

Peer reviewed version

A Robust Half-Cycle Single-Phase Pre-Filtered Open-Loop Frequency Estimator for Fast Tracking of Amplitude and Phase

Anant Kumar Verma, *Member, IEEE,* Pedro Roncero-Sánchez, *Senior Member, IEEE,* Hafiz Ahmed, *Senior Member, IEEE,* Seifeddine Ben Elghali, and Tiago Davi Curi Busarello, *Member, IEEE*

***Abstract*—This paper presents a fast phase-locking and amplitude detection scheme for single-phase applications. The proposed scheme employs a pseudo-rectification process in order to generate even harmonics from the grid signal. The DC-offset component present in the grid signal increases the sensitivity of the pseudo-rectification process, and the design of the pre-filtering stage must, therefore, be completely focused on the rejection of DC-offset and the even-harmonics. The application of a half-cycle pre-filter would consequently appear to be a highly attractive option as regards improving the dynamic response time and even harmonic rejection abilities. However, the elimination of the DC-offset component and the estimation of phase and amplitude information is still a very challenging task. The aforementioned issues are addressed by employing a half-cycle comb filter and a half-cycle non-adaptive Lyapunov orthogonal signal generator. The estimation of single-phase grid parameters is thereby made simpler by employing an improved open-loop frequency estimation, which is capable of providing accurate frequency deviation information with good precision. The research shown herein also reveals that the estimation of the amplitude and phase information differs slightly from the usual mathematical notations owing to the pseudo-rectification method adopted in the proposed work. Note that the pre-filtering stage is non-adaptive in nature, which may lead to steady-state errors in the amplitude and phase information under off-nominal frequency conditions. An online mathematical correction approach dependent on frequency deviation is, therefore, employed in order to obtain the error-free amplitude and phase information. Finally, the robustness of the current proposal is validated by experimentally comparing several known grid parameter estimation schemes using a real-time controller.**

***Index Terms*—Frequency estimation, half-cycle comb filter, moving average filter, orthogonal signal generation, single-phase grid voltage.**

I. Introduction

PHASE-locking is an essential and necessary phenomenon that is frequently utilised when synchronising electronic measurement systems [1], power electronic converters (PECs) connected to the utility grid [2] and/or the active-power filters employed in aerospace applications [3]. In an electrical power system network, the best-known control algorithms that are most appropriate for the control of PECs are phase-locked loops (PLLs) [4]-[6] and frequency-locked loops (FLLs) [7], [8], which are responsible for rapidly providing the phase and the frequency information, respectively. Furthermore, the higher penetration of renewable energy sources into the utility grid impacts on the inertial component of the grid [9]. The recent grid codes are, therefore, modified in order to place emphasise on the rapid detection of the fundamental amplitude in order to accommodate fault ride-through capability and to obtain precise frequency information under weak inertia grid conditions so as to enhance grid resilience and power system stability [9]–[11].

The ongoing research initiatives with respect to the known PLL and FLL techniques are limited by a major challenge concerning the design of an effective pre-filtering technique that can be applied in order to generate harmonic and DC-offset-free fundamental orthogonal signals (FOCs) [12]. In a single-phase system, an improved dynamic response of a synchronisation algorithm relies principally on the rapid extraction of FOCs. The filter attribute, i.e. the window length, decides how long the dynamic response will take to estimate the FOCs while eliminating the negative effects of DC-offset and odd-harmonic components present in the grid signal. The filtering approaches are sub-categorised as in-loop filtering techniques [13] and pre-loop filtering techniques [14], [15]. The selection of any filtering stage differs according to the PLLs and FLLs chosen, which are implemented in a synchronous reference frame (dq) [16] and a stationary reference frame ($\alpha\beta$) [17], respectively. It is, therefore, suggested that the filtering stages chosen should be appropriate in order to target and properly eliminate the challenging grid voltage disturbances.

The extensive works related to PLLs indicate that the DC-offset and harmonics will yield full-cycle and even-harmonic components in the $dq-$frame, which may affect the accuracy of an estimation algorithm [18]. The most prominent filters, such as moving average filters (MAFs) [19] and delayed signal cancellation operators [20], are, therefore, a very attractive option when attempting to handle these disturbances. However, their limitation concerns the window length of the filter, which must be equivalent to one fundamental period in order to effectively eliminate the negative effects of the DC-offset component [21]. Note that significant delays often lead to a poor dynamic performance of PLLs. The phase lead compensation approach is a suitable means to avoid delays at the expense of an increase in the computational load and tedious controller tuning [22].

Open-loop synchronisation schemes (OLSs) are, meanwhile, equally appealing owing to their structural simplicity and easy implementation when compared to the known PLL and FLL techniques [23]. Their beauty lies in the combination of non-adaptive pre-filtering stages, along with open-loop frequency estimators [21], [23]-[28], [30] whose operating principles are similar to those of FLLs, i.e. they lock the frequency information rather than the phase information obtained from the voltage at the point of common coupling. The best-known frequency estimators are the discrete oscillator law (DOL) [24]-[26] and the "Teager energy operator (TEO)" [27], [28]. However, these frequency estimators alone are incapable of handling the DC-offset and harmonics present in the grid

signal [27]. Filters such as interpolation based filters [24], [30], recursive discrete Fourier transform (RDFT) [27], half-cycle RDFT [26] [28], the MAF-based orthogonal signal generator (OSG) [25], demodulation approaches [25], [29], [30], the error demodulation based OSG [6], [21], or second-order generalised integrator (SOGI) filters [7], [23], are, therefore, employed for this purpose.

Another prominent aspect of an OLS is its capacity to avoid the frequency feedback-loop, which helps to obtain a better dynamic response when compared to PLLs. Of the aforementioned pre-filtering approaches, the half-cycle RDFT combined with DOL is a very efficient approach with which to accurately estimate the frequency in less than one fundamental cycle. However, there are no proper solutions with which to solve issues such as the DC-offset present in the grid signal and the estimation of amplitude and phase information when half-cycle filters are deployed [26]. In this proposal, a better solution is provided in order to address the concerns regarding the fast tracking of amplitude and phase information with the help of half-cycle filters. A good immunity towards DC-offset and harmonics may be simultaneously attained with the current arrangement of the proposed pre-filtering stage by employing a pseudo-rectification approach. Moreover, the combination of an improved open-loop frequency estimator with the proposed filtering stage allows the effective elimination of the errors in the amplitude and phase without adding significant delay to the estimation, in addition to providing the frequency estimation with good precision.

II. Impacts of Pseudo-Rectification on Single-Phase Signal

The well-known instrumentation and measurement techniques established through the use of precise voltage and current sensors make it possible to feed a compatible grid voltage and/or current signal to an estimation algorithm embedded in real-time hardware. The concept of pseudo-rectification states that a single-phase sinusoidal signal sensed from the point of common coupling can be mathematically rectified inside digital hardware for the purpose of generating even harmonics [24]. The pseudo-rectification process can, therefore, be studied in the following steps and by treating the fundamental grid voltage signal as expressed below:

$$v_g(t) = A_1 \sin \underbrace{(\Omega_1 t + \Phi_1)}_{\Theta_1} \tag{1}$$

where, A_1, Ω_1, Φ_1 and Θ_1 are the fundamental amplitude, the fundamental angular grid frequency (rad./s), the initial phase (rad.) and the fundamental phase (rad.), respectively. The pseudo-rectified grid signal can be expressed as follows:

$$v_r(t) = v_g^2(t) = A_1^2 \sin^2(\Omega_1 t + \Phi_1) \tag{2}$$

Note that Equation (2) is further exploited by applying trigonometric identity, i.e. $\sin^2(\theta) = \frac{1-\cos(2\theta)}{2}$, as follows:

$$v_r(t) = \underbrace{\frac{A_1^2}{2}}_{V_p} - \underbrace{\frac{A_1^2 \cos(2\,\Omega_1 t + 2\,\Phi_1)}{2}}_{\text{Second Harmoic Component}} \tag{3}$$

The major drawback of (3) is the presence of an unavoidable pseudo DC-offset component (V_p) that needs to be effectively handled by the filtering stage. It is possible to take leverage from the pseudo-rectification approach, as the grid frequency of interest will eventually become twice the fundamental angular grid frequency, i.e. $2\Omega_1$. Moreover, the odd-harmonics of interest will become even-harmonics, signifying that the half-cycle (HC) filters are beneficial as regards eliminating the negative effects of even harmonics. Note that HC filters are not immune to the DC-offset component present in the grid signal. Moreover, the negative effect of an actual DC-offset component present in the grid signal is not effectively addressed by the pseudo-rectification method.

A. Impact of the actual DC-offset component present in the single-phase grid signal

Some of the issues that may contaminate the grid voltage signal with the DC-offset (V_o) component are the signal conditioning units, analogue-to-digital conversion circuitry, or the saturation of transformers etc. The signal $v_g(t)$ in (1), which is contaminated with V_o, is, therefore, expressed as:

$$v_g^{'}(t) = v_g(t) + V_o \tag{4}$$

The rectification process, if re-applied to (4), yields:

$$v_r^{'}(t) = (v_g^{'}(t))^2 = v_g^2(t) + 2v_g(t)V_o + V_o^2 \tag{5}$$

Equation (5) is then re-written as follows:

$$v_r^{'}(t) = v_r(t) + 2v_g(t)V_o + V_o^2 \tag{6}$$

Upon expanding (6) and re-collecting the terms, a very challenging DC-offset issue will appear, as expressed below:

$$v_r^{'}(t) = \underbrace{V_o^2 + V_p}_{\text{DC-offset}} - \frac{A_1^2}{2}\cos(2\,\Theta_1) + \underbrace{2V_o A_1 \sin(\Theta_1)}_{v_f(t)} \tag{7}$$

It can be inferred that the presence of V_o will severely affect the dynamic performance of an estimation algorithm when a pseudo-rectification method is adopted, since the rejection of components, i.e. V_o^2 and $2V_o A_1 \sin(\Theta_1)$, requires additional efforts when designing the filters. Moreover, the component '$v_f(t)$' explains that the DC-offset component will yield fundamental oscillations with a magnitude of $2V_o * A_1$. Full-cycle (FC) filters are required in order to reject these disturbances [21]. In addition to dealing with these concerns several works in literature effectively adopt an HC-filter rather than an FC-filter when the fundamental frequency of interest is '$2\Omega_1$' [26]. One of the possible advantages of employing HC-filters is, moreover, an improvement to the dynamic response time of any estimation algorithm. However, HC-filters are not very attractive owing to the fact that they are incapable of rejecting the V_o component present in the grid signal.

B. Impact of the harmonic component present in the single-phase grid signal

The non-linear power electronic loads connected to the utility grid are responsible for harmonic pollution and the

This article has been accepted for publication in IEEE Transactions on Instrumentation and Measurement. This is the author's version which has not been fully edited and content may change prior to final publication. Citation information: DOI 10.1109/TIM.2021.3129211

degradation of power quality. A third harmonic component ($v_3(t) = A_3\sin(3\Theta_1)$) is considered in (1), as follows:

$$v_g^{''}(t) = v_g(t) + v_3(t) \tag{8}$$

Upon applying a mathematical square operation to Equation (8), the aforementioned study reveals that when the grid signal is contaminated with odd-harmonics, then the pseudo-rectification process will yield even harmonics, as follows:

$$v_r^{''}(t) = (v_g^{''}(t))^2 = (A_1\sin(\Theta_1) + A_3\sin(3\Theta_1))^2 \tag{9}$$

Upon expanding Equation (9), we obtain:

$$v_r^{''}(t) = A_1^2\sin^2(\Theta_1) + A_3^2\sin^2(3\Theta_1) + 2A_1A_3\sin(\Theta_1)\sin(3\Theta_1) \tag{10}$$

Equation (10) is then re-written as follows:

$$v_r^{''}(t) = v_r(t) + \frac{A_3^2}{2} - \frac{A_3^2\cos(6\Theta_1)}{2} + A_1A_3\Big[\cos(2\Theta_1) - \cos(4\Theta_1)\Big] \tag{11}$$

Note that $v_r^{''}(t)$ is affected only by even harmonic components and that an HC-filter could, therefore, be employed owing to its good ability to reject the even harmonic components. In the current proposal, an attempt is made to develop a single-phase grid synchronisation scheme based on HC-OSG for the estimation of the fundamental grid voltage parameters.

III. Proposed Half-cycle Pre-filtering Stage

In this section, the major challenge as regards V_o is handled by including an HC-comb filter prior to the pseudo rectification process. Furthermore, an HC-non-adaptive OSG is proposed in order to reject the negative effects of the pseudo DC-offset (V_p) and the even harmonic components.

A. Half-cycle pre-filter for pre-rejection of V_o

As discussed in Section II-A, the DC-offset (V_o) component present in the grid signal may yield two components when the pseudo-rectification method is adopted, i.e.

- V_o^2
- $v_f(t) = 2V_o\ A_1\ \sin(\Theta_1)$

The elimination of these components is very challenging when it is necessary to leverage the benefits of HC-OSGs. Note that these components are induced owing to the mathematical square operation applied to the grid signal. An HC-comb filter is, therefore, deployed prior to the pseudo-rectification process. The discrete time grid voltage signal contaminated with the V_o and the third harmonic component is expressed as follows for quantitative understanding:

$$v_h(n) = \underbrace{A_1\sin(\Omega_1 nT_s + \Phi_1)}_{v_g(n)} + \underbrace{A_3\sin(3\Omega_1 nT_s + \Phi_1)}_{v_3(n)} + V_o \tag{12}$$

where n and T_s are the sampling instant and the sampling time, respectively. The signal delayed by $N/2$ samples is,

$$v_h(n - \frac{N}{2}) = v_g(n - \frac{N}{2}) + v_3(n - \frac{N}{2}) + V_o \tag{13}$$

where $N = T_w/T_s$ is the number of samples and $T_w = 2\pi/\Omega_1$. The grid voltage signal free-from V_o can be obtained as follows:

$$v_e(n) = v_h(n) - v_h(n - \frac{N}{2}) \tag{14}$$

Upon solving equation (14), the DC-offset component is completely rejected without affecting the odd-harmonics present in the grid signal, as shown below:

$$v_e(n) = 2A_1\sin(\Omega_1 nT_s + \Phi_1) + 2A_3\sin(3\Omega_1 nT_s + \Phi_1) \tag{15}$$

In order to ensure that the information regarding odd-harmonics remains unchanged, the signal $v_e(n)$ must be divided by a factor of 1/2, and the transfer function of the HC-comb filter is obtained as follows:

$$C(z) = V_e(z)/V_g(z) = (1 - z^{-\frac{N}{2}})/2 \tag{16}$$

For qualitative analysis, at nominal angular grid frequency ($\Omega_1 = \Omega_o$ where $\Omega_o = \frac{2\pi}{T_o}$ rad/s, $T_o = \frac{1}{f_o}$; $f_o = 50$ Hz) in Fig. 1(a), a grid voltage signal contaminated with 0.3 p.u. DC-offset and the odd-harmonics (i.e. $h = 3, 5, 7, 9, 11, 13, 15, 17$), as per the EN 50160 [32] standard (Fig. 1(b)) is considered. A good DC-offset rejection ability

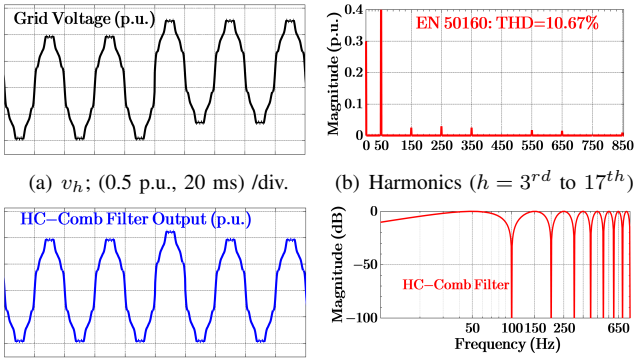

(a) v_h; (0.5 p.u., 20 ms) /div. (b) Harmonics ($h = 3^{rd}$ to 17^{th})

(c) $v_e(n)$; (0.5 p.u., 20 ms) /div. (d) Frequency response plot

Fig. 1. DC-offset rejection capability of a HC-comb filter.

without affecting the odd-harmonics within 0.5 times of the fundamental cycle can be observed in Fig. 1(c). Furthermore, the HC-comb filter is ideally suited to addressing the concerns induced by 'V_o', as exemplified in Fig. 1(d), owing to its ability to by-pass the odd-harmonics without any attenuation and the complete rejection of the DC-offset component present in the grid signal.

B. Half-cycle OSG for elimination of even-harmonics

In the block diagram of the proposed pre-filtering stage depicted in Fig. 2, when a signal labelled $u(n)$ follows a pseudo-rectification process, it generates even harmonics similar to the process discussed in Section II-B. The signal labelled $v_i(n)$ is subsequently affected by following disturbances:

- DC-offset: $V_{po} = \sum_{i=1,3,..}^{M} \frac{A_i^2}{2}$
- Even harmonic terms i.e. $\sum_{i=3,5..} E_i(2\Omega_1)$

In this case, the fundamental input signal of interest is:

$$v_2(n) = -\frac{A_1^2\ \cos(2\ \Omega_1 nT_s + 2\ \Phi_1)}{2} \tag{17}$$

The input signal to the HC-OSG structure can be re-written in a simplified manner as follows:

$$v_i(n) \equiv v_2(n) + \sum_{i=3,5..} E_i(2\Omega_1) + V_{po} \tag{18}$$

This article has been accepted for publication in IEEE Transactions on Instrumentation and Measurement. This is the author's version which has not been fully edited and content may change prior to final publication. Citation information: DOI 10.1109/TIM.2021.3129211

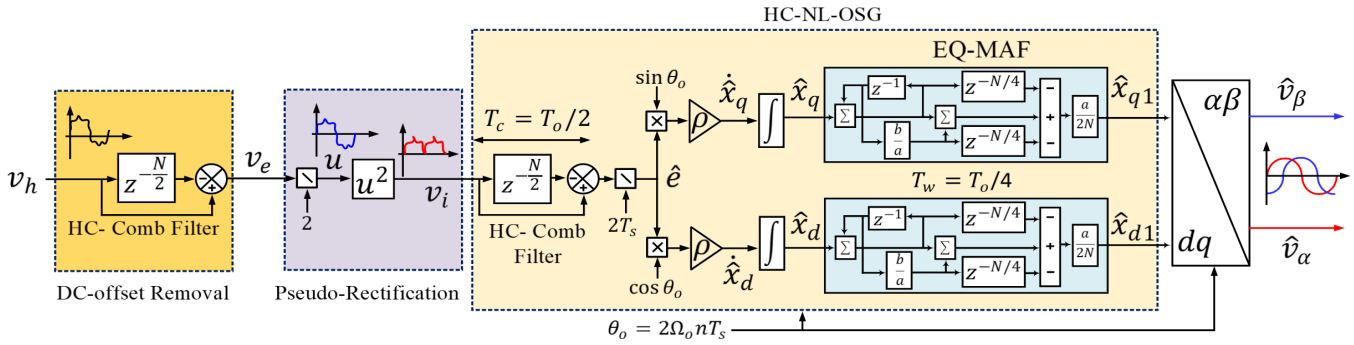

Fig. 2. General block diagram of the proposed pre-filtering stage.

An HC non-adaptive Lyapunov theory based-OSG (HC-NL-OSG) approach is, therefore, applied, which acts as a band-pass filter for the cumulative rejection of the DC-offset component (V_{po}) and the even-harmonics components ($E(2\Omega_1)$) when the fundamental frequency is twice the actual frequency of interest, i.e. $2\Omega_1$.

1) Pseudo DC-offset (V_{po}) rejection: In order to eliminate the negative effect of V_{po}, let us, for the sake of simplicity, consider a grid voltage signal without ($E(2\Omega_1)$), as follows:

$$v_i(n) = v_2(n) + V_{po} \tag{19}$$

The signal delayed by $N/2$ samples is:

$$v_i(n - N/2) = v_2(n - N/2) + V_{po} \tag{20}$$

As shown in Fig. 2, it is possible to employ another HC-comb filter with a window length of $T_c = T_o/2$, in order to effectively reject the V_{po} component, which also helps to obtain an error signal, as expressed below:

$$\hat{e} = \frac{v_i(n) - v_i(n - N/2)}{2T_s} = \frac{v_2(n) - v_2(n - N/2)}{2T_s} \tag{21}$$

Equation (21) is expressed as follows:

$$\hat{e} = \frac{-A_1^2 \cos(2\,\Omega_1 n T_s + 2\Phi_1) + A_1^2 \cos(2\,\Omega_1 n T_s + 2\Phi_1 - N\Omega_1 T_s)}{4T_s} \tag{22}$$

Note that the error signal must tend towards zero if $\Omega_1 = \Omega_o$.

2) Even harmonic ($E(2\Omega_1)$) rejection: Lyapunov's estimation law [21] suggests that the $dq-$frame components, as observed in the pre-filtering stage, can be estimated once the error signal has been obtained from (22), as follows:

$$\dot{\hat{x}}_q(n) = \frac{\hat{x}_q(n) - \hat{x}_q(n-1)}{T_s} = \rho\, \hat{e} \sin(\overbrace{2\Omega_o n T_s}^{\theta_o})\, T_s \tag{23}$$

$$\dot{\hat{x}}_d(n) = \frac{\hat{x}_d(n) - \hat{x}_d(n-1)}{T_s} = \rho\, \hat{e} \cos(2\Omega_o n T_s)\, T_s \tag{24}$$

where the constant gain ρ is a fixed value and is expressed as $\rho = 16 f_o$. The state variables defined in Equations (23) and (24) are valid only when the fundamental component of $2\Omega_1$ is present in $v_i(n)$. In the case of the presence of a third harmonic component in the grid signal, the equivalent even harmonic component is expressed as follows:

$$E_3(2\Omega_1) = -\frac{A_3^2 \cos(6\Theta_1)}{2} + A_1 A_3 \Big[\cos(2\Theta_1) - \cos(4\Theta_1)\Big] \tag{25}$$

The grid voltage signal is, therefore, expressed as:

$$v_i(n) = v_2(n) + E_3(2\Omega_1) \tag{26}$$

The grid signal expressed in (26) can be routed through the comb filter, and after applying Lyapunov's estimation law, the generic state variables can be expressed as follows:

$$\dot{\hat{x}}_q(n) = \rho\, \hat{e} \sin(2\Omega_o t)\, T_s + \rho\, E_3(2\Omega_1) \sin(2\Omega_o t)\, T_s \tag{27}$$

$$\dot{\hat{x}}_d(n) = \rho\, \hat{e} \cos(2\Omega_o t)\, T_s + \rho\, E_3(2\Omega_1) \cos(2\Omega_o t)\, T_s \tag{28}$$

It can be understood that the even harmonics will be completely eliminated with the help of an HC-cycle comb filter alone at $2\Omega_1 = 2\Omega_o$. However, under off-nominal frequency conditions, in order to achieve a good attenuation of even harmonics, an enhanced zero phase-delay quarter-cycle MAF (EQMAF) [15] with a window length of $T_w = T_o/4$ is, therefore, employed in the $dq-$frame so as to obtain filtered $\hat{x}_{q1}$ and $\hat{x}_{d1}$ components without any additional phase-lag. The parameters, i.e. a and b are denoted as $(N+1)/N$ and $(1-N)/N$, respectively. In Fig. 3, the magnitude curve below

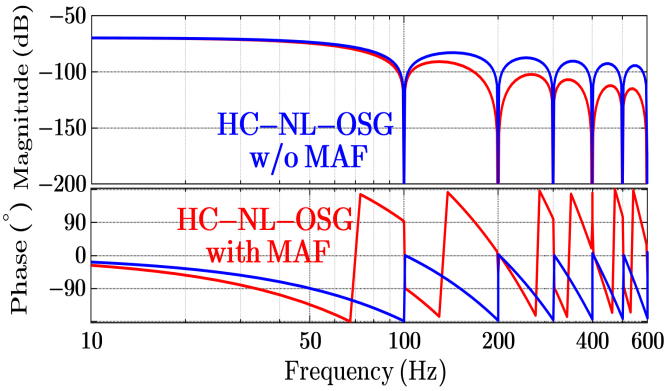

Fig. 3. Bode plot of HC-NL-OSG with and without MAF.

-50 dB in the bode response plot indicates that the fundamental amplitude information will be lost in the output of the HC-NL-OSG. Furthermore, the frequency response characteristics are sufficiently shaped to provide the even harmonics with a better attenuation by involving EQMAF in the OSG structure. The dynamic response time of HC-NL-OSG with and without EQMAF is shown in Fig. 4. Note that the time taken by the HC-NL-OSG when considering EQMAF is 15 ms. The total time that the proposed pre-filtering stage takes to obtain the

This article has been accepted for publication in IEEE Transactions on Instrumentation and Measurement. This is the author's version which has not been fully edited and content may change prior to final publication. Citation information: DOI 10.1109/TIM.2021.3129211

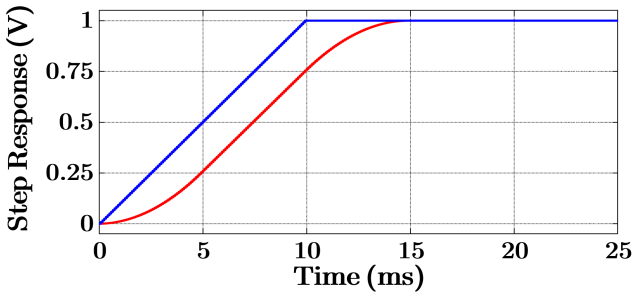

Fig. 4. Step response of HC-NL-OSG in the presence of MAF (red) and the absence of MAF (blue).

fundamental orthogonal signals at 50 Hz when considering the HC-comb filter employed before the pseudo-rectification process is the following:

$$T_p = 10\text{ms} + 10\text{ms} + 5\text{ms} = 25\text{ms} \tag{29}$$

The amplitude and the phase information of the fundamental grid voltage component may be affected during the process of pseudo-rectification. It should be noticed that the proposed pre-filtering stage is non-adaptive. Thus, the error correction in the fundamental amplitude and phase is still required once the frequency deviation information is known [21], [30].

IV. Improved Fundamental Frequency Estimator

An enhanced and modified frequency estimation technique like that reported in [21] and which relies on the storage of two grid voltage samples is now re-investigated. The involvement of a robust adaptive law makes it possible to obtain an accurate estimate of the frequency deviation. Insights into the known TEO are also emphasized in this section. The frequency estimation law is, therefore, expressed as follows:

$$\hat{x}^*_\alpha(n)\,\hat{x}^*_\alpha(n-N) + \hat{x}^*_\beta(n)\,\hat{x}^*_\beta(n-N) = \cos\left(N\Omega_1 T_s\right) \tag{30}$$

where the unit $\alpha\beta-$frame signals ($\hat{x}^*_\alpha(n)$, $\hat{x}^*_\beta(n)$) are,

$$\begin{aligned}\hat{x}^*_\alpha(k) &= \frac{X_\alpha}{\sqrt{\hat{x}^2_\alpha + \hat{x}^2_\beta}}\sin\left(n\,\Omega_1\,T_s\;+\;\phi\right)\\ \hat{x}^*_\beta(k) &= \frac{X_\beta}{\sqrt{\hat{x}^2_\alpha + \hat{x}^2_\beta}}\cos\left(n\,\Omega_1\,T_s\;+\;\phi\right)\end{aligned} \tag{31}$$

where, X_α and X_β, Ω_1, ϕ, T_s, and n are the fundamental magnitude of the $\alpha\beta-$frame components, the angular grid frequency deviation, the initial phase and the sampling period, respectively. Let us define a signal M_1, as expressed below:

$$M_1 = \hat{x}^*_\alpha(n)\,\hat{x}^*_\alpha(n-N) + \hat{x}^*_\beta(n)\,\hat{x}^*_\beta(n-N) \tag{32}$$

where the distance between two samples is denoted by 'N'. Equation (30) can be re-written using a trigonometric identity ($\sin(\theta) = \sqrt{(1-\cos(2\theta))/2}$), as follows:

$$\sqrt{\frac{1-M_1}{2}} = \sin\left(\frac{N\Omega_1 T_s}{2}\right) \tag{33}$$

Equation (33) requires only two consecutive samples in order to estimate the fundamental frequency deviation, as follows:

$$\hat{f}_1 = \frac{1}{N\pi T_s}\arcsin\left(\sqrt{\frac{1-M_1}{2}}\right) \tag{34}$$

The fundamental frequency is estimated as follows:

$$\Delta\hat{f}_1 = \hat{f}_1/2 - f_o \tag{35}$$

where, f_o is the nominal frequency (i.e. 50 Hz). The factor '1/2' is considered owing to the even fundamental component, i.e. 100 Hz. The reason for obtaining (33) in this manner is to provide a new insight into the well-known TEO by re-writing the term '1' as follows:

$$\left(\hat{x}_\alpha(n-1)\right)^2 + \left(\hat{x}_\beta(n-1)\right)^2 = 1 \tag{36}$$

Upon employing, (32), (33), (36), N= 2, and without considering amplitude normalisation, Equation (33) could be reverse engineered, thus indicating that the well-known TEO can be applied to both components of the $\alpha\beta-$axes, as follows:

$$\left(\hat{x}_\alpha(n-1)\right)^2 - \hat{x}_\alpha(n)\,\hat{x}_\alpha(n-2) = \sin^2(\Omega_1 T_s) \tag{37}$$

$$\left(\hat{x}_\beta(n-1)\right)^2 - \hat{x}_\beta(n)\,\hat{x}_\beta(n-2) = \sin^2(\Omega_1 T_s) \tag{38}$$

Research suggests that two TEOs can be employed, one with the $\alpha-$axis and the other with the $\beta-$axis. Upon adding (37) and (38), the simplified form of the fundamental frequency estimator similar to (34) is obtained as follows:

$$\hat{f}_1 = \frac{1}{2\pi T_s}\arcsin\left(\sqrt{\frac{\hat{x}_\alpha(n-1))^2+\hat{x}_\beta(n-1))^2-M_1}{2}}\right) \tag{39}$$

In (37)–(39), note that six samples are stored in the memory of a real-time controller in order to obtain the fundamental frequency. However, in (34), it can be inferred that the sample storage ability of the TEO can be enhanced by simply utilising unit orthogonal signals. Furthermore, for the un-attenuated harmonic disturbances (i.e. $D(n)$) in the $\alpha\beta-$frame, the estimated fundamental angular frequency is expressed as follows:

$$\hat{\Omega}_h = \frac{2}{NT_s}\arcsin\left(\sqrt{\frac{1-M_h+D(n)}{2}}\right) \tag{40}$$

where, subscript 'h' denotes the order of harmonic components. A better robustness and an improved accuracy in the estimate of frequency under off-nominal frequency conditions is achieved by adopting a robust adaptive law [33] in order to handle the negative effect of $D(n)$, and the output error is expressed as follows:

$$\hat{e}_1(n) = \sin^2\left(\frac{N\hat{\Omega}_1 T_s}{2}\right) - \frac{1-M_1+D(n)}{2} \tag{41}$$

Substituting (33) in (41) yields,

$$\hat{e}_1(n) = \sin^2\left(\frac{N\hat{\Omega}_1 T_s}{2}\right) - \sin^2\left(\frac{N\Omega_1 T_s}{2}\right) - \frac{D(n)}{2} \tag{42}$$

If $x(n) = \sin^2\left(\frac{N\Omega_1 T_s}{2}\right)$, and is substituted in (42), we obtain,

$$\hat{e}_1(n) = \hat{x}(n) - x(n) - \frac{D(n)}{2} \tag{43}$$

The robust adaptive law is, therefore, expressed as follows:

$$\hat{x}(n+1) = \hat{x}(n) - \lambda\left[\frac{\hat{x}(n)-\hat{e}(n)}{1+\hat{e}^2(n)}\right] - \gamma\hat{x}(n) \tag{44}$$

The term "$\gamma\hat{x}(n)$" is obtained from the σ-modification method [34], which may provide robustness with respect to $D(n)$,

This article has been accepted for publication in IEEE Transactions on Instrumentation and Measurement. This is the author's version which has not been fully edited and content may change prior to final publication. Citation information: DOI 10.1109/TIM.2021.3129211

where $\gamma \in \left[0, 10^{-5}\right)$ and $\lambda \in \left(10^{-2}, 1\right]$ are the adaptive gains whose limits are obtained using rigorous simulation results. The estimated frequency deviation is expressed as follows:

$$\frac{\hat{f}_1}{2} = \frac{1}{2N\pi T_s} \arcsin\left[\sqrt{\frac{\hat{x}(n)}{2}}\right] \tag{45}$$

If N=2 is chosen, the estimated grid frequency deviation is:

$$\Delta\,\hat{f}_1 = \frac{1}{4\pi T_s} \arcsin\left[\sqrt{\frac{\hat{x}(n)}{2}}\right] - f_o \tag{46}$$

where f_o is 50 Hz. Note that if $\Omega_1 \neq \Omega_o$, then $X_\alpha \neq X_\beta \neq A$, and as a consequence, oscillations are observed in $\Delta\hat{f}_1$ and the adaptive law alone is incapable of handling this issue if it is necessary to maintain a fast dynamic response. Note that the lower values of 'γ' help to accurately attain the mean value of the estimated frequency, whereas lower values of 'λ' help to control the dynamic behaviour, as exemplified in Fig. 5. There is, consequently a trade-off between the steady-state

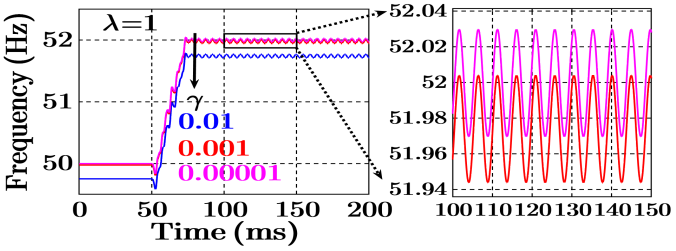

(a) Estimated frequency for different values of γ.

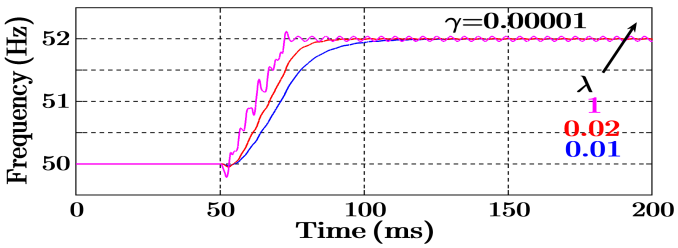

(b) Estimated frequency for different values of λ.

Fig. 5. Comparison of steady-state accuracy.

accuracy and the dynamic response when the values of λ and γ are varied. From the analysis carried out in Fig. 5, it can be understood that the impact of 'γ' is negligible on the estimate of the fundamental frequency. Thus, the choice of $\gamma = 0$ allows maximizing the mean value tracking ability of the adaptive law with minimum tuning gain parameters. As indicated by the dotted line in Fig. 6, the feedback path formed by the tuning gain parameter is no more required. Hence, the adaptive law expressed in (46) can be rewritten as follows:

$$\hat{x}(n+1) = \hat{x}(n) - \lambda\left[\frac{\hat{x}(n) - \hat{e}(n)}{1 + \hat{e}^2(n)}\right] \tag{47}$$

Thus, the estimated frequency deviation is:

$$\Delta\,\hat{f}_1 = \frac{1}{4\pi T_s} \arcsin\left[\sqrt{\frac{\hat{x}(n+1)}{2} + \frac{\lambda}{2}\left[\frac{\hat{x}(n) - \hat{e}(n)}{1+\hat{e}^2(n)}\right]}\right] - f_o \tag{48}$$

Further, the choice of parameter '$\lambda = 1$' has provided a fast dynamic response in the estimate of frequency, as observed in Fig. 5(a). However, the choice of $\lambda = 1$ eliminates the low-pass filtering capability of the adaptive law. Thus, additional filtering is required to attenuate the off-nominal steady-state ripples in the estimated frequency. An HC-MAF with a window length of $T_m = T_o/2$ is, therefore, eventually deployed to attenuate the steady-state oscillations in the estimated frequency while considering $\gamma = 0$ and $\lambda = 1$, as shown in Fig. 6. Nevertheless, the lower values of 'λ' provide good low-pass filtering capability but at the expense of slower dynamic response, as depicted in Fig. 5(b). This is advantageous as the transient overshoots in frequency may be minimized without any additional low-pass filter under weak inertia grid conditions. Another control parameter that is associated with the proposed frequency estimator is the sampling time (T_s) interval, whose effects are shown in Fig. 7. Note

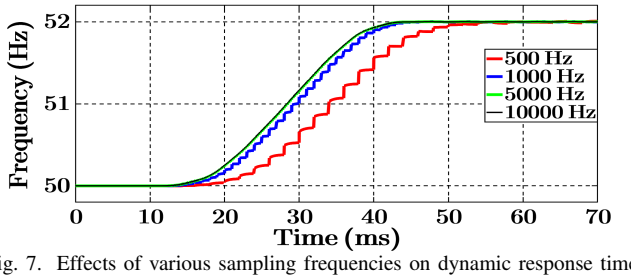

Fig. 7. Effects of various sampling frequencies on dynamic response time.

that the low sampling frequency operation, i.e. $f_s \leq 10 f_o$ Hz, will yield a slower dynamic response. Furthermore, $f_s \geq 20 f_o$ Hz, will provide an accurate convergence time, as computed in the proposed work. The proposed scheme can, therefore, be employed with low-cost embedded hardware if $f_s > 20 f_o$ Hz criterion is met in order to set the sampling frequency 10 to 100 times faster than the system's internal frequency. On the other hand, the difference between the steady-state frequency errors and the transient performance at 5 kHz and 10 kHz is comparable as evident from Table I.

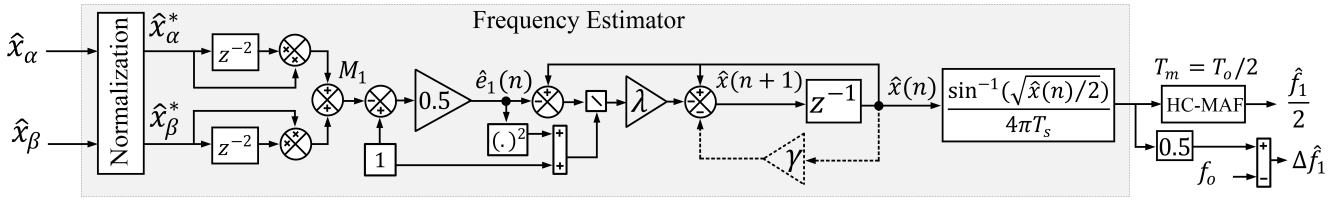

Fig. 6. Proposal with which to estimate the fundamental frequency deviation.

This article has been accepted for publication in IEEE Transactions on Instrumentation and Measurement. This is the author's version which has not been fully edited and content may change prior to final publication. Citation information: DOI 10.1109/TIM.2021.3129211

TABLE I
SIMULATED DATA FOR STEADY-STATE ERRORS AND TRANSIENT RESPONSE TIME AT DIFFERENT SAMPLING FREQUENCIES

f_s \ $\Delta f_1 \rightarrow$	-3	-2	1	0	1	2	t_r (ms)	Resolution
500 Hz	18	12	6	0	5.74	10	≈80	Poor
1000 Hz	15.2	7	1.4	0	1.5	7	40	Good
5000 Hz	8	2.56	0.3	0	0.3	2.24	35	Better
10000 Hz	8	2.55	0.3	0	0.3	2.24	35	Better
	Steady-State Frequency Error (mHz)							

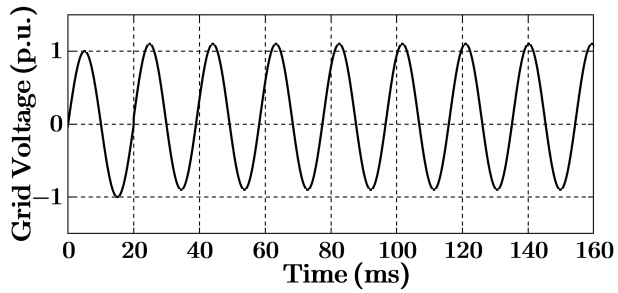

(a) Harmonically distorted grid voltage signal with DC-offset.

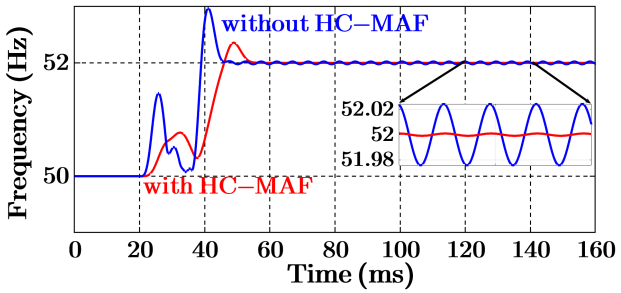

(b) Estimation of +2 Hz frequency step, i.e., 50-52 Hz.

Fig. 8. Frequency step tracking performance in the presence of 10% of DC-offset component.

For a low cost application, the choice of 5 kHz sampling frequency may be preferred to further reduce the computations and utilized the allocated memory space in an embedded hardware efficiently. For this purpose, the designer can always recompute the number samples as per the system's internal frequency. Hence, the proposed scheme is easily deployable on a low-cost microcontroller. The ability to attenuate the state-state ripples and to effectively estimate the frequency with a negligible amount of error in the presence of a 10% DC-offset component in the grid signal, which was obtained in the simulation environment, is presented in Fig. 8.

Nevertheless, the frequency estimation suffers from steady-state errors due to the non-adaptive nature of the pre-filtering stage. However, these steady-steady errors are well below the acceptable limit. Moreover, the proposed scheme takes 35 ms to accurately track the large positive (see Fig. 9) and negative frequency deviations in the presence of harmonics in the grid signal (see Fig. 10). The proposed frequency estimator has good steady-state accuracy with a negligible error in the estimate of frequency, as depicted in Fig. 11. Note that the maximum error observed under off-nominal frequency

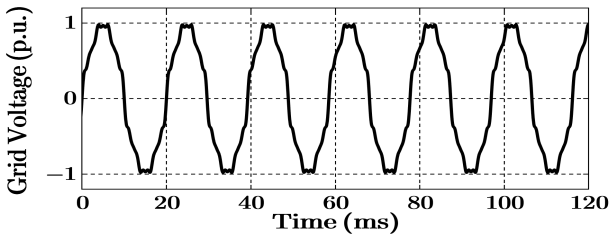

(a) Grid voltage signal

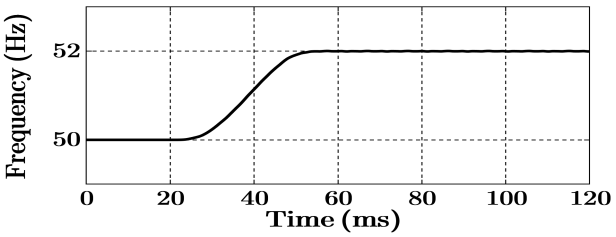

(b) Estimated frequency

Fig. 9. Positive frequency deviation in the presence of harmonics.

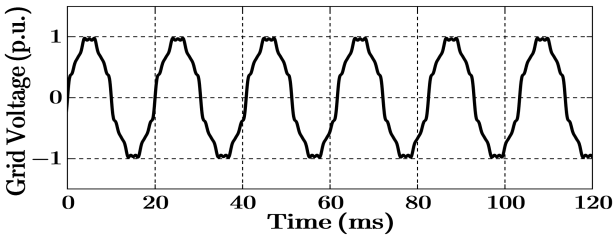

(a) Grid voltage signal

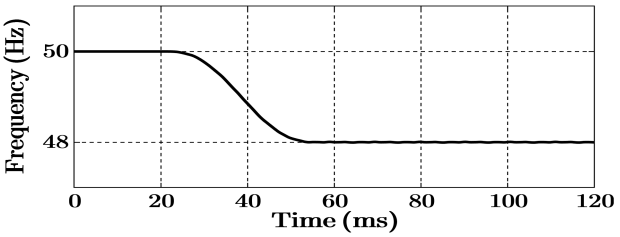

(b) Estimated frequency

Fig. 10. Negative frequency deviation in the presence of harmonics.

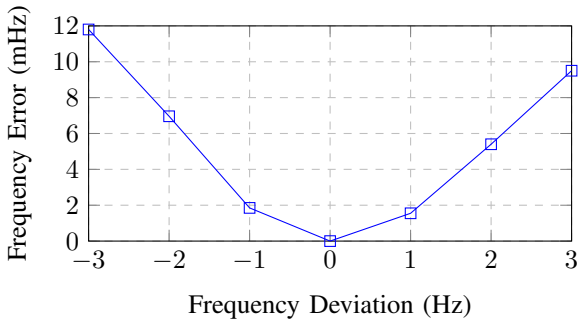

Fig. 11. Frequency error observed in the presence of hamonics.

conditions in the presence of harmonics is below 12 mHz, which complies with the IEC 61000-4-7 standard in which the maximum permissible error is below 15 mHz [27], [31]. The proposed frequency estimator is, therefore, a suitable choice for instruments that require good frequency precision.

V. Detection of Amplitude and Phase Angle

The detection of fundamental amplitude and phase information continues to be a challenging issue with even harmonic generation schemes. With the current proposal, it is possible to obtain the amplitude and phase information accurately. The fundamental orthogonal signals are expressed as follows:

$$\hat{x}_\alpha = -A_1^2 \sin(2\,\Omega_1 n T_s + 2\,\Phi_1) \tag{49}$$

$$\hat{x}_\beta = -A_1^2 \cos(2\,\Omega_1 n T_s + 2\,\Phi_1) \tag{50}$$

The factor '1/2' in (49) and (50) has already been nullified by the multiplying factor considered in the constant gain ρ, i.e. $\mathbf{2} * 8f_o$. The mathematical square operation is subsequently applied to both sides of the equations (49) and (50) as follows:

$$\hat{x}_\alpha^2 = A_1^4 \sin^2(2\,\Omega_1 n T_s + 2\,\Phi_1) \tag{51}$$

$$\hat{x}_\beta^2 = A_1^4 \cos^2(2\,\Omega_1 n T_s + 2\,\Phi_1) \tag{52}$$

Upon adding (51) and (52), the fundamental amplitude is:

$$A_1 = \sqrt[4]{\hat{x}_\alpha^2 + \hat{x}_\beta^2} \tag{53}$$

Upon using (49) and (50), the fundamental phase angle information is obtained as follows:

$$\Theta_1 = \frac{1}{2}\arctan\left(\frac{\hat{x}_\alpha}{\hat{x}_\beta}\right) \tag{54}$$

Note that both the amplitude and phase information will be inaccurate owing to the fixed frequency architecture of the pre-filtering stage. An error correction technique [21], [30] is, therefore, employed to eliminate the errors in the estimation of fundamental amplitude and phase angle information. This is achieved by developing the amplitude and phase angle compensation gains as a function of Δf_1. First, an amplitude compensation factor is determined, which is a dimensionless fraction of 1 p.u. to A_1, and is defined as follows:

$$A_u = 1/A_1 \tag{55}$$

The errors in the fundamental amplitude can be eliminated by observing the values of A_u for every step change in the input supply frequency from 47 to 52 Hz, i.e. 1 Hz per step, as shown in Table II. The compensation factor is expressed as a quadratic function of $\Delta\hat{f}_1$, as shown below:

$$A_u = 0.0004\,(\Delta\hat{f}_1)^2 + 0.000005\,(\Delta\hat{f}_1) + 1.0628 \tag{56}$$

The coefficients in (56) are obtained from the curve shown in Fig. 12. The phase error is similarly calculated offline for the input supply frequency variation in steps and the errors are noted, as shown in Table II.

TABLE II
Data for Amplitude and Phase Compensation Gains

Δf_1 (Hz)	-3	-2	-1	0	1	2
K_c (rad.)	0.5515	0.6295	0.7074	0.7853	0.8634	0.9415
A_u	1.06666	1.064395	1.063264	1.0629	1.06326	1.064509

The phase compensation gain is subsequently expressed as follows:

$$K_c = 0.078(\Delta\hat{f}_1) + 0.7854 \tag{57}$$

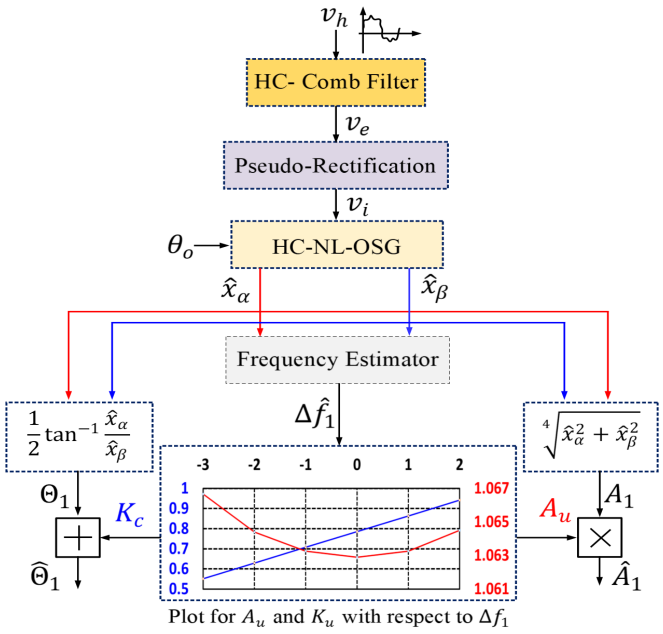

Fig. 12. Detailed flow chart of the proposed scheme.

The coefficients in (57) are obtained from the plot shown in Fig. 12. Note that Equations (56) and (57) are updated online in a feed-forward manner once the information regarding $\Delta\hat{f}_1$ has been obtained from (48). The actual fundamental amplitude is:

$$\hat{A}_1 = A_1 * A_u \tag{58}$$

The actual phase angle information is similarly:

$$\hat{\Theta}_1 = \Theta_1 + K_c \tag{59}$$

The directional flow chart of the proposed technique is, therefore, provided in Fig. 12 in order to correlate the fact that the estimation of the grid parameters remains open-loop in nature.

VI. Experimental Results

In this section, the proposed scheme is compared with well-known techniques such as the demodulation based PLL (D-PLL) [6], an improved SOGI based OLS [23] and the MAF based OLS [25] by utilizing the experimental test bench, as shown in Fig. 13. The grid voltage signal measured, i.e. 1

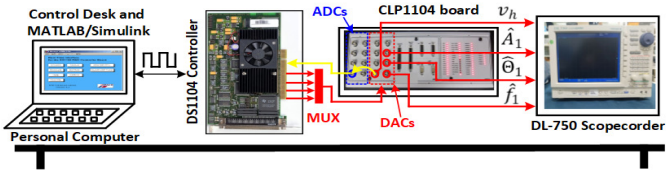

Fig. 13. Experimental test bench.

p.u. can be generated internally through the use of a digital-to-analogue converter (DAC) port of a dSPACE (DS1104) controller card, which is sampled at 10 kHz. The codes complied for the different control algorithms implemented in a MATLAB/Simulink environment using a discrete time solver are also simultaneously burned into the memory of the

This article has been accepted for publication in IEEE Transactions on Instrumentation and Measurement. This is the author's version which has not been fully edited and content may change prior to final publication. Citation information: DOI 10.1109/TIM.2021.3129211

DS1104. The control algorithms will receive a grid voltage signal through an analogue-to-digital converter (ADC) port, while the grid parameters will be obtained from DACs, which are captured on a DL-750 Scopecoder.

Comparisons of Amplitude, Phase and Frequency Tracking:

The D-PLL, SOGI-OLS, MAF-OLS schemes and that proposed herein have been identified by employing colours, i.e. pink, red, blue and green, respectively. In Fig. 14(a)-14(f), the grid voltage is subjected to a 50% voltage sag in the presence of harmonics at 50 Hz and a frequency step of +2 Hz in the presence of 0.3 p.u. of DC-offset. The corresponding estimated

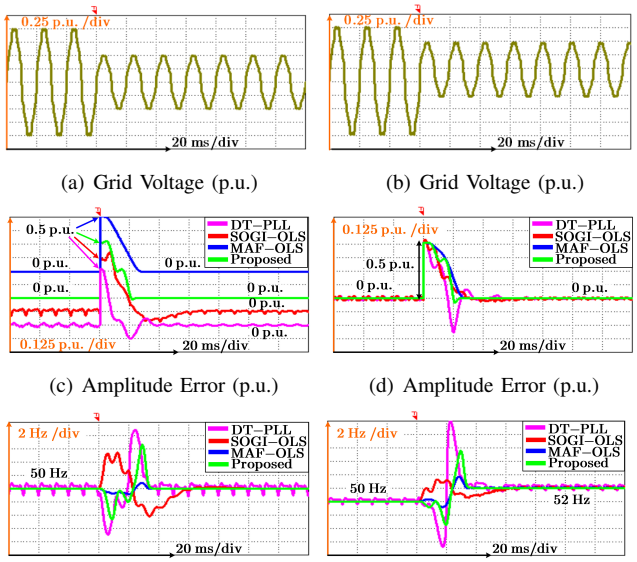

(a) Grid Voltage (p.u.) (b) Grid Voltage (p.u.)

(c) Amplitude Error (p.u.) (d) Amplitude Error (p.u.)

(e) Estimated Frequency (50 Hz) (f) Frequency (50-52 Hz)

Fig. 14. Amplitude tracking performance at 50 Hz and 50-52 Hz.

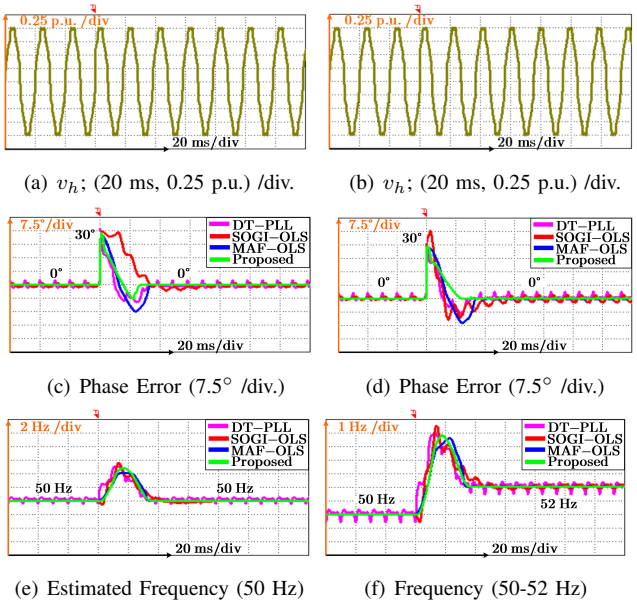

(a) v_h; (20 ms, 0.25 p.u.) /div. (b) v_h; (20 ms, 0.25 p.u.) /div.

(c) Phase Error (7.5° /div.) (d) Phase Error (7.5° /div.)

(e) Estimated Frequency (50 Hz) (f) Frequency (50-52 Hz)

Fig. 15. Phase tracking performance at 50 Hz and 50-52 Hz.

amplitude errors and the details of frequency information are presented in Fig. 14(c) and Fig. 14(d), Fig. 14(e) and

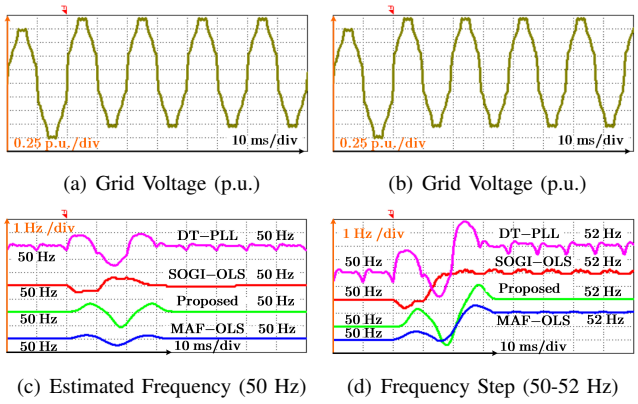

(a) Grid Voltage (p.u.) (b) Grid Voltage (p.u.)

(c) Estimated Frequency (50 Hz) (d) Frequency Step (50-52 Hz)

Fig. 16. DC-offset rejection capability.

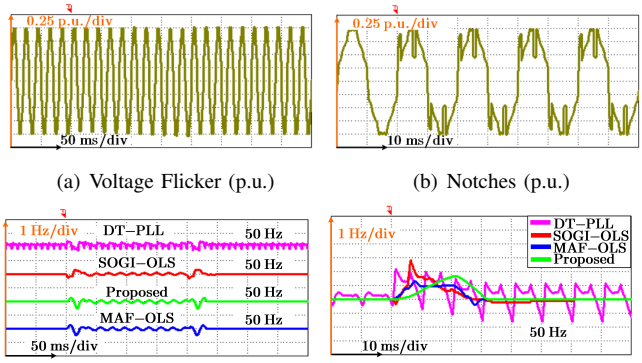

(a) Voltage Flicker (p.u.) (b) Notches (p.u.)

(c) Estimated Frequency (Hz) (d) Estimated Frequency (Hz)

Fig. 17. Frequency tracking performance in the presence of voltage flicker and the notches in the supply voltage.

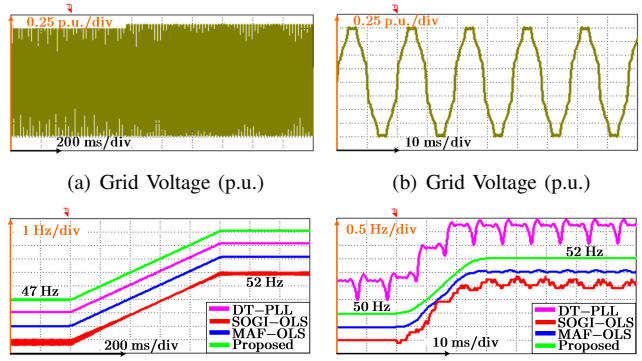

(a) Grid Voltage (p.u.) (b) Grid Voltage (p.u.)

(c) Frequency Ramp (47-52 Hz) (d) Frequency Step (50-52 Hz)

Fig. 18. Frequency ramp and step tracking performances.

Fig. 14(f), respectively. Note that the proposed scheme is able to provide amplitude information within 20 ms when compared to all the other schemes, with good immunity towards DC-offset and harmonics. However, the overshoot in frequency is large when compared to that of ISOGI-OLS and MAF-OLS. The proposed scheme estimates frequency with good precision in a response time of 35 ms. The phase tracking performance in the presence of harmonics at nominal frequency and under off-nominal frequency conditions is presented in Fig. 15(a)-15(f). A fast dynamic response of 25 ms is obtained with the proposed scheme when compared to all the other schemes. Note that all the schemes are capable of tracking the changes in

frequency and phase. Higher precision is obtained with the current proposal as regards the estimation of phase and frequency. Apart from this, the phase and the amplitude information are independent of the computations done within the proposed frequency estimator. Therefore, a better dynamic response is obvious in the case of amplitude and phase estimation under off-nominal frequency conditions. Since, the steady-state errors present in the estimate of frequency have a negligible impact on the accuracy of phase and amplitude information. In order to ensure a better DC-offset rejection capability under both nominal and off-nominal frequency conditions, two test cases are provided in Fig. 16(a)-16(d). A good immunity to DC-offset and improved precision are observed in the case of the proposed frequency estimator, with a dynamic response time of 35 ms. The immunity to a triangular voltage flicker of ± 1 p.u., 2.5 Hz and notches in the supply voltage is similarly observed in Fig. 17(a)-17(d). Note that all the OLSs, including the proposed scheme, are capable of handling the notches and voltage flickers present in the grid voltage supply when compared to D-PLL. The frequency ramp and the frequency step abilities are, meanwhile, shown in Fig. 18(a)-18(d). It is worth mentioning that all the schemes are capable of tacking these changes. However, the ISOGI-OLS and the D-PLL have poor dynamic responses when compared to those of MAF-OLS and the proposed scheme. A better harmonic rejection ability under off-nominal frequency conditions is also observed in the case of the current proposal. Finally, a precise phase tracking PLL (HIHD-PLL [5]) algorithm and various synchronisation schemes are compared with the proposed scheme, and the data obtained is presented in Table III. Note that the proposed scheme (phase jump 30°) and the HIHD-PLL (phase jump -10°) are able to track the phase information within 25 ms and 20.1 ms, respectively. In the case of grid voltage sag, a comparable dynamic performance is achieved by the MAF-OLS and the proposed technique. However, a peak overshoot in the estimate of frequency is found to be comparable in the case of DT-PLL and the proposed scheme. Moreover, the DT-PLL has a very accurate phase angle tracking performance under the off-nominal frequency condition when compared to the other schemes. Furthermore, the HIHD-PLL and MAF-OLS schemes behave similarly in terms of phase preciseness. Nevertheless, the proposed scheme has better preciseness as regards phase and dynamic response. The positive and negative frequency deviation (Δf) tracking ability in the case of HIHD-PLL has different types of dynamic behaviour [5]. Note that both the proposed and the other schemes have similar dynamic behaviour as regards $\pm\Delta f$ tracking. The proposed scheme is, therefore, suitable for converters operating in weak inertia grids and the low voltage ride through (LVRT) applications.

TABLE III
PERFORMANCE COMPARISON

Case	Peak Errors	Synchronization Schemes			
		DT-PLL	MAF-OLS	HIHD-PLL	Proposed
Voltage Sag (50%)	Δf_p (Hz)	≈4	≈0.4	≈0.53(99%)	≈3
	t_r (ms)	≈40	≈33	-	≈35
+2 Hz Positive Δf	Δf_p (Hz)	-	0	0	0
	t_r (ms)	≈30	≈30	≈62	≈30
Phase Jump (30°)	θ_p (Hz)	0°	0°	4.12(-10°)	0°
	t_r (ms)	≈30	≈30	≈20.1	≈25
Off-nominal Phase Error (10^{-3}rad.)		0	<70	<10	<1.2
DC-offset Rejection		Yes	Yes	Yes	Yes
Harmonic Rejection		Poor	Good	Better	Better
Steady-State Accuracy		Low	High	High	High
$\pm\Delta f$ Tracking		Equal	Equal	Unequal	Equal
Inter-Harmonic Rejection		Poor	Good	Good	Good
Control parameters		3	1	3	2

Math Functions	DT-PLL	MAF-OLS	HIHD-PLL	Proposed
Trignometric	0	2	2	2
Inverse Trignometric	1	2	0	2

VII. CONCLUSION

This paper shows a proposal for a pseudo-rectification based single-phase open-loop frequency estimation scheme that helps to obtain the fast tracking of fundamental amplitude and phase information. The combination of a half-cycle comb-filter and a half-cycle non-adaptive Lyapunov-based OSG helps to address the issues, i.e. the DC-offset and harmonics, present in the grid voltage signal. A better immunity is achieved when compared to the known single-phase even-harmonic generation schemes that are employed only for frequency estimation. The harmonic and DC-offset free estimation of orthogonal signals within 25 ms assists in the rapid extraction of amplitude and phase information. Moreover, the proposed pre-filtering stage makes it possible to effectively obtain all the grid voltage parameters, i.e. amplitude, phase and frequency, within 1.75 times of the fundamental period. The combination of the proposed filtering stage with an improved open-loop frequency estimator helps to eliminate steady-state errors in the fundamental amplitude and phase information with better precision. Note that selecting the control parameters as $\lambda = 1$ and $f_s = 10$ kHz makes it possible to control the dynamic response behaviour of the estimated frequency within 35 ms. Of all these critical parameters, the low sampling frequency operation such as $f_s \leq 10 f_o$ Hz yields sluggish dynamic behaviour, and the choice of sampling must, therefore, be considered as $f_s > 20 f_o$ Hz for better precision and dynamic behaviour. The comparative experimental results clearly show the effectiveness of the current proposal as regards its suitability for synchronising single-phase grid connected converters employed in weak inertia grids, in addition to meeting LVRT requirements.

REFERENCES

[1] F. M. Gardner, "Phaselock techniques," *IEEE Transactions on Systems, Man, and Cyber.*, vol. SMC-14, no. 1, pp. 170-171, Jan.-Feb. 1984.

[2] M. G. Simões, F. Harirchi, and M. Babakmehr, "Survey on time-domain power theories and their applications for renewable energy integration in smart-grids," *IET Smart Grid*, vol. 2, no. 4, pp. 491–503, Dec. 2019.

[3] J. F. Guerreiro, J. A. Pomilio and T. Davi Curi Busarello, "Design and implementation of a multilevel active power filter for more electric aircraft variable frequency systems," *Brazilian Power Electronics Conference*, Gramado, Brazil, 2013, pp. 1001-1007

[4] S. Golestan, J. M. Guerrero, and J. C. Vasquez, "Single-phase PLLs: a review of recent advances," *IEEE Trans. Power Electron.*, vol. 32, no. 12, pp. 9013–9030, Dec. 2017.

[5] Z. Ali, N. Christofides, L. Hadjidemetriou, E. Kyriakides, "Design of an advanced PLL for accurate phase angle extraction under grid voltage HIHs and DC offset," *IET Power Electron.*, vol. 11, no. 6, pp. 995-1008, Dec. 2017.

[6] H. Ahmed and M. Benbouzid,"Demodulation type single-phase PLL with DC offset rejection," *IET Electron. Letters*, vol. 56, no. 7, pp. 344–347, Apr. 2020.

[7] J. Yu, W. Shi, J. Li , L. Deng, and M. Pei, "A discrete-time non-adaptive SOGI-based frequency-locked loop," *IEEE Trans. Power Systs.*, vol. 35, no. 6, pp. 4912–4915, Nov. 2020.

[8] H. Ahmed and M. Benbouzid, "On the enhancement of generalized integrator-based adaptive filter dynamic tuning range," *IEEE Trans, on Instrum. and Meas.*, vol. 69, no. 10, pp. 7449–7457, Oct. 2020.

[9] M. Saeedian *et al.*, "Enhancing frequency stability of weak grids with modified distributed virtual inertia method," *IEEE 11th International Symposium on Power Electronics for Distributed Generation Systems (PEDG)*, pp. 187-192, Nov. 2020.

[10] E. Afshari *et al.*, "Control strategy for three-phase grid-connected PV inverters enabling current limitation under unbalanced faults," *IEEE Trans. Indus. Electron.*, vol. 64, no. 11, pp. 8908-8918, Nov. 2017.

[11] "IEEE Recommended Practice for Voltage Sag and Short Interruption Ride-Through Testing for End-Use Electrical Equipment Rated Less than 1000 V," *IEEE Std 1668-2017 (Revision of IEEE Std 1668-2014)*, pp.1-85, 27 Nov. 2017

[12] Y. Han, M. Luo, X. Zhao, J. M. Guerrero, and L. Xu, "Comparative performance evaluation of orthogonal-signal-generators-based single-phase PLL algorithms–A survey," *IEEE Trans. Power Electron.*, vol. 31, no. 5, pp. 3932–3944, May. 2016.

[13] M. Karimi-Ghartemani, S. A. Khajehoddin, P. K. Jain, and A. Bakhshai, "Derivation and design of in-loop filters in phase-locked loop systems," *IEEE Trans. Instrum. Meas.*, vol. 61, no. 4, pp. 930–940, Apr. 2012.

[14] S. Golestan, J. M. Guerrero, A. Vidal, A. G. Yepes and J. Doval-Gandoy, "PLL with MAF-based prefiltering stage: small-signal modeling and performance enhancement," *IEEE Trans. on Power Electron.*, vol. 31, no. 6, pp. 4013–4019, Jun. 2016.

[15] L. Ibarra, D. Guillen, J. Aviles, P. Ponce, and A. Molina, "A Fourier-based phasor estimator with a modified MAF and its application in distribution networks," *IEEE Trans. on Indus. Inform.*, Early Access, Feb. 2021.

[16] S. Golestan, E. Ebrahimzadeh, B. Wen, J. M. Guerrero and J. C. Vasquez, "dq-Frame Impedance Modeling of Three-Phase Grid-Tied Voltage Source Converters Equipped With Advanced PLLs," *IEEE Trans. on Power Electron.*, vol. 36, no. 3, pp. 3524–3539, Mar. 2021

[17] S. Golestan, J. M. Guerrero, M. J. H. Rawa, A. M. Abusorrah and Y. Al-Turki, "FLLs in electrical power and energy systems: equivalent or different to PLLs ?," *IEEE Indus. Electron. Mag.*, Feb. 2021.

[18] N. Hui, Y. Feng, and X. Han, "Design of a high performance phase-locked loop with DC offset rejection capability under adverse grid condition," *IEEE Access*, vol. 8, pp. 6827–6838, Jan. 2020.

[19] W. Luo and D. Wei, "A frequency-adaptive improved moving-average-filter-based quasi-type-1 PLL for adverse grid conditions," *IEEE Access*, vol. 8, pp. 54145–54153, Mar. 2020.

[20] D. S. S. Andrade, Y. N. Batista, F. A. S. Neves, H. E. P. de Souza, "Fast phase angle jump estimation to improve the convergence time of the GDSC-PLL," *IEEE Trans. Ind. Electron.*, vol. 67, no. 4, pp. 2852–2862, May 2020.

[21] A. K. Verma, C. Subramanian, R. K. Jarial, P. Roncero-Sánchez and U. M. Rao, "A robust Lyapunov's demodulator for tracking of single-/three-phase grid voltage variables," *IEEE Trans. on Instrum. and Meas.*, vol. 70, pp. 1-11, Dec. 2021.

[22] S. Gautam, Y. Lu, W. Hassan, W. Xiao, and D. D.-C. Lu, "Single phase NTD PLL for fast dynamic response and operational robustness under abnormal grid condition," *Electr. Power Syst. Res.*, vol. 180, Mar. 2020.

[23] H. Ahmed, S. Biricik, and Md. Benbouzid, "Low-pass filtering or gain tuning free simple DC offset rejection technique for single and three-phase systems," *Elect. Power Syst. Res.*, vol. 186, May 2020.

[24] P. Roncero-Sanchez, X. del Toro Garcia, A. P. Torres, and V. Feliu, "Robust frequency-estimation method for distorted and imbalanced three-phase systems using discrete filters," *IEEE Trans. Power Electron.*, vol. 26, no. 4, pp. 1089–1101, Apr. 2011.

[25] S. Golestan, J. M. Guerrero, and J. C. Vasquez, "An open-loop grid synchronization approach for single-phase application," *IEEE Trans. Power Electron.*, vol. 33, no. 7, pp. 5548–5555, Jul. 2018.

[26] M. S. Reza, M. M. Hossain, and V. G. Agelidis, "Fast and accurate frequency estimation in distorted grids using a three-sample based algorithm," *IET Gener. Transm. Distrib.*, vol. 13, no. 18, pp. 4242–4248, Aug. 2019.

[27] M. S. Reza and V. G. Agelidis, "Single-phase grid voltage frequency estimation using Teager energy operator-based technique," *IEEE J. Emerg. Sel. Topics Power Electron.*, vol. 3, no. 4, pp. 1218–1227, Dec. 2015.

[28] M. S. Reza, M. M. Hossain, and M. Ciobotaru, "Teager energy operator for fast estimation of three-phase grid frequency," *IEEE Trans. Ins. Meas.*, Early Access, Sept. 2020.

[29] C. A. G. Marques, M. V. Ribeiro, and E. A. B. Da Silva, "Enhanced demodulation-based technique for estimating the parameters of fundamental component in power systems," *IET Gener. Transm. Distrib.*, vol. 5, no. 9, pp. 979–988, Sep. 2011.

[30] M. S. Reza and V. G. Agelidis, "A demodulation-based technique for robust estimation of single-phase grid voltage fundamental parameters," *IEEE Trans. Ind. Informat.*, vol. 13, no. 1, pp. 166–175, Feb. 2017.

[31] *Testing and Measurement Techniques General Guide on Harmonics and Interharmonics Measurements and Instrumentation for Power Supply Systems and Equipment Connected Thereto,* 2002.

[32] *Voltage Characteristics of Electricity Supplied by Public Distribution Systems*, Eur. Std. EN 50160, 2008.

[33] H. Wang, Y. Yang, D. Chen, X. Ge, S. Li and Y. Zuo, "Speed-sensorless control of induction motors with an open-loop synchronization method," *IEEE J. Emerg. Sel. Topics in Power Electron.*, Early Access, Jan. 2021.

[34] G. Tao, *Adaptive Control Design and Analysis*. Hoboken, NJ, USA: Wiley, 2003.

Anant Kumar Verma (S'16-M'19) obtained his bachelor degree in Instrumentation Engineering from University Science Instrumentation Center Srinagar, India in 2012. He obtained his master's degree from Dehradun Institute of Technology (DIT), Dehradun, India in 2014. He is currently pursuing the Ph.D. degree in Electrical Engineering from National Institute of Technology, Hamirpur.

His research interests include renewable energy systems, modeling of grid synchronization algorithms, and control of power electronic converters.

Pedro Roncero-Sánchez (M'07-SM'14) received an M.Sc. degree in electrical engineering from Universidad Pontificia Comillas, Madrid, Spain, in 1998, and a Ph.D. degree from the University of Castilla-La Mancha, Ciudad Real, Spain, in 2004. He is currently an Associate Professor at the School of Industrial Engineering, University of Castilla-La Mancha. His research interests include control of power electronic converters, power quality, renewable energy systems, energy storage devices and wireless power transfer.

Hafiz Ahmed (Senior Member, IEEE) received the PhD degree in Automatic Control from the University of Lille 1, Villeneuve-d'Ascq, France, in 2016. From 2016 to 2021, he was with Clemson University (South Carolina, USA), Asia Pacific University (Dhaka, Bangladesh), North South University (Dhaka, Bangladesh), Coventry University (Coventry, UK), and Birmingham City University (Birmingham, UK). Since April 2021, he has been with the Nuclear Futures Institute, Bangor University, UK, where he is the Sêr Cymru Senior Lecturer (Associate Professor) in Nuclear Instrumentation and Control. His current research interests include applied control engineering with special focus in energy and environment.

Dr. Ahmed was the recipient of the European Embedded Control Institute (EECI) PhD Award in 2017 and Best PhD Theses Award from the Research Cluster on Modelling, Analysis, and Management of Dynamic Systems (GDR-MACS) of the National Council of Scientific Research (CNRS) in France, in 2017. He is an Associate Editor for the International Journal of Electrical Engineering and Education. He is also actively involved in organizing special issues and sessions at various international journals and conferences.

This article has been accepted for publication in IEEE Transactions on Instrumentation and Measurement. This is the author's version which has not been fully edited and content may change prior to final publication. Citation information: DOI 10.1109/TIM.2021.3129211

Seifeddine Ben Elghali received the B.Sc. degree in Electrical Engineering in 2005 from ENIT, Tunis, Tunisia, the M.Sc. degree in Automatic Control in 2006 from the University of Poitiers, Poitiers, France, and the Ph.D. degree in Electrical Engineering in 2009 from the University of Brest, Brest, France. After receiving the Ph.D. degree, he joined the French Naval Academy, Brest, France as a Teaching and Research Assistant. Since 2010, he is an Associate Professor of Electrical Engineering at Aix-Marseille University, Marseille, France. His current research interests include modeling and control of renewable energy applications.

Tiago Davi Curi Busarello is a professor at the Federal University of Santa Catarina (UFSC) - Campus Blumenau, Brazil, since 2016. He obtained the PhD and the Msc in Electrical Engineering at the University of Campinas (UNICAMP), Brazil, in 2015 and 2013 respectively. He obtained the bachelor degree in Electrical Engineering from the Santa Catarina State University in 2010, Brazil. In 2014, he was a visitor researcher at Colorado School of Mines, USA. He is a member of the IEEE (Institute of Electrical and Electronics Engineers) and he is associated with IEEE Power Electronics Society and Brazilian Power Electronics Society (SOBRAEP). Areas of interest: Power Electronics, control for power electronics, digital signal processing for power electronics.